Chapter 5

Role of Entrainment and Added Mass in Propulsive Performance

5.1 Introduction

Results for the propulsive performance studies in chapter 4 show that increases in propulsive efficiency are generated for the vehicle in the pulsed jet mode of propulsion in comparison to the steady jet mode of propulsion. This chapter investigates the fluid mechanics that contribute to the increased propulsive performance. Section 5.2 describes the experimental procedures and conditions that existed during the laser Doppler velocimetry trials. Section 5.3 describes the relationship of nozzle-exit overpressure to the hydrodynamic impluse. Section 5.4 investigates the role of ambient fluid entrainment in a developing vortex as a potential source of increased propulsive performance. Jet velocity profiles were measured and presented in section 5.4.1 and are used to obtain a measure of the entrainment ratio discussed in section 5.4.2. Added mass effect is another potential source for increased propulsive performance. A model developed by Krueger (2001) is used in section 5.5 to determine the fraction of the total impulse imparted to the flow that is contributed by added mass. A model was developed in section 5.6 to investigate how the increase in total fluid impulse due to vortex ring formation relates to the propulsive efficiency. The model was applied in section 5.6 to estimate the propulsive efficiency for the pulsed jet configuration at three motor speeds.

5.2 Experimental Conditions

The ambient fluid entrainment into the jet was measured for two motor speeds in the steady jet configuration and three motor speeds in the pulsed jet configuration. To decrease the load on the motor, the steady jet experiments were conducted without the inner rotating shell. It was shown in chapter 4 that the behavior of the jet is similar for both the steady jet with and without the rotating shell. One series of steady jet experiments was conducted with a motor speed of 2900 $\pm$ 30 rpm, producing an average jet speed of 154 $\pm$ 38 cm/s and a Re_j of 69,950. Another set of experiments was conducted with a motor speed of 3160 $\pm$ 40 rpm, generating an average jet speed of 157 $\pm$ 38 cm/s and a Re_j of 71,400. In order to make accurate comparisons between both modes of propulsion, comparable motor speeds were obtained for the series of pulsed jet experiments. The first set of experiments were conducted at the lowest motor speed able to sustain steady vehicle speed. These pulsed jet experiments were conducted at a motor speed of 2750 $\pm$ 30 rpm, generating an average jet speed of 142 $\pm$ 30 cm/s and a Re_j of 64,400. The steady jet configuration was unable to maintain a constant body velocity at the corresponding motor speed, therefore, no steady jet experiments were available for comparison at the lowest motor speed. The second set of pulsed jet experiments were conducted at 2970 $\pm$ 30 rpm, producing an average jet speed of 149 $\pm$ 30 cm/s and a Re_j of 67,400. The last set of experiments were performed at a motor speed of 3200 $\pm$ 30 rpm, producing an average jet speed of 158 $\pm$ 32 cm/s.

Given that laser Doppler velocimetry provides a pointwise measurement of the jet speed, it was necessary to translate the measurement probe to obtain a velocity profile as illustrated in figure 5.1. Given that the jet is axisymmetric, the probe volume was programmed to obtain speed measurements of the axial component of the velocity starting at the jet center. Measurements where obtained in 2 mm increments moving in the x direction up to a distance of x/D = 1. See figure 5.1. The y position was kept constant and the z position was fixed at 0.5 inches away from the jet exit. Given the velocity range of the vehicle and the 30 m maximum vehicle translation distance in the facility, the velocity profile could not be captured in a single trial. An entire velocity profile was captured in 4 to 6 segments. Each segment consists of measuring the velocity at 3 to 6 radial positions.

Approximately 3 to 5 seconds of data was captured at each radial position. To reduce measurement noise and error, two to four trials were conducted for each segment of the velocity profile. The miniLDV is capable of measuring only a single component of velocity at a given instant in time. Due to this limitation, the probe was rotated by 90^o to obtain measurements of the speed in the x direction (i.e., radial velocity) and the procedure was repeated. Approximately 18 trials under the same experimental conditions, including motor speed and starting position, were necessary to complete the velocity profile for a given motor speed.

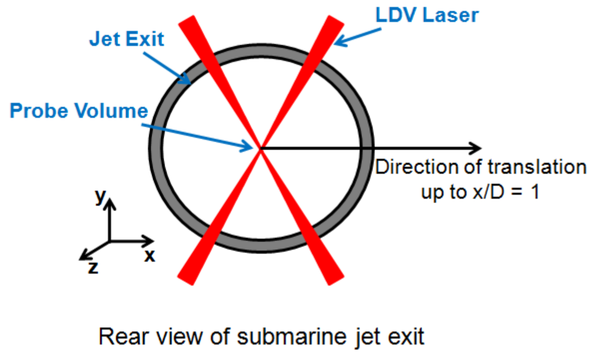

Figure 5.1. Schematic illustrating the translation of the LDV probe volume.

5.3 Relationship of Nozzle-Exit Overpressure to the Hydrodynamic Impulse

The total impulse in the flow, I(t), has been shown to increase by Krueger and Gharib (2003) with the presence of vortex ring formation due to nozzle-exit overpressure. The nozzle-exit overpressure is associated with the acceleration of the ambient fluid by vortex ring formation in the form of added mass and entrained mass. Through a control volume analysis of the fluid region external to the jet exit, it can be shown that the impulse injected into the flow by the jet is determined by a flux term and a contribution from overpressure as described in Krueger (2001), resulting in equation (5.1),

$$I(t) = I_U(t) + I_p(t), \tag{5.1}$$

where $I_U(t)$ is the total impulse due to the jet momentum flux and $I_p(t)$ is the pressure-impulse.

Krueger (2001) defines the total impulse of the flow, I(t), as the following,

$$I(t) = I_U(t) + I_p(t) = (m_{ejected} + m_{entrained} + M)W, \tag{5.2}$$

where $m_{ejected}$ is the mass of fluid that is ejected from the nozzle, $m_{entrained}$ is the mass of the ambient fluid entrained into the vortex ring, and the third component is the added mass of the vortex, M. These three classes of fluid move at the mean velocity of the vortex ring, W. A schematic of a fully developed vortex ring illustrating the three different masses of moving fluid is shown in figure 1.1. Krueger states that the momentum of the ejected fluid ($m_{ejected}\,W$) is derived from the jet momentum, I_U, and not from I_p. As a result, I_p is only associated with $(m_{entrained} + M)\,W$, and contributes only to the acceleration of ambient fluid in the form of added and entrained mass.

5.4 Relationship of Entrainment to Improved Propulsive Performance

As discussed in section 5.3, one benefit of vortex ring formation for propulsion is the entrainment of ambient fluid into the developing vortex ring. The entrained fluid must be accelerated with the vortex thus increasing the impulse supplied by the jet (Krueger and Gharib 2003). The velocity profile of the jet was measured in order to obtain an entrainment ratio. The entrainment ratio is defined by equation (5.3),

$$\frac{Q}{Q_o} = \frac{\int_0^{2\pi} \int_0^{r_o} U_z(r) dr\, d\theta}{U_{avg}\, A_j}, \tag{5.3}$$

where Q is the total volumetric flow rate defined by the integration under the blue and red curve illustrated in figure 5.2. Q_o is the volumetric flow rate through the jet exit and is represented by the integration under the blue curve simplifying to the product of U_{avg} and A_j. The entrainment ratio was calculated at two motor speeds in the steady jet configuration and three motor speeds in

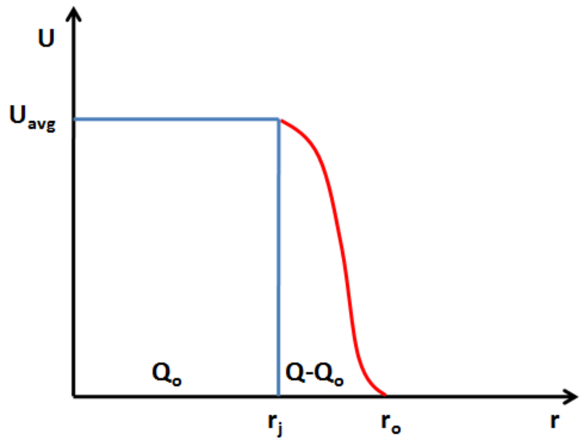

Figure 5.2. Entrainment ratio.

the pulsed jet configuration to investigate the role of entrainment.

5.4.1 Comparison of Velocity Profiles Obtained Using LDV

5.4.1.1 Comparison of Velocity Profiles for Uz

Figure 5.3 shows the axial velocity profiles for three motor speeds. The average axial velocity, U_z, was normalized by the average jet velocity, U_{avg}, and was plotted against a normalized distance x/r. A top hat profile was obtained for both the steady and pulsed jet modes of propulsion and for all motor speeds tested. For the given axial position of z/D = 0.25, these profiles are similar to the work of Reynolds et al. (2003) and Ho and Gutmark (1987). As the jet speed increases, the velocity outside the jet nozzle, x/r > 1.0, decreases rapidly to zero as noted by the smaller values of U_z/U_{avg} for both modes of propulsion. The magnitude of the velocity outside the jet is greater for the pulsed jet in comparison to the steady jet for a given equivalent jet speed suggesting greater fluid entrainment due to vortex ring formation.

The root-mean-square velocity fluctuation in U_z, w′, is normalized by U_{avg} and plotted against x/r in figure 5.4. The velocity fluctuations are greater inside the jet in comparison to the fluctuations in the free stream. Results from the pulsed jet experiments shown in figure 5.4(a) and figure 5.4(c) display two distinct peaks, one at x/r = 0.5 and the other near the jet exit of x/r = 1. The results in figure 5.4(b) show a turbulent fluctuation peak near the jet exit for both the steady and unsteady modes of propulsion.

5.4.1.2 Comparison of Velocity Profiles for Ux

Figure 5.5 shows the velocity profiles of U_x for three motor speeds. The average velocity of U_x is normalized by the average jet velocity U_{avg} and plotted against a normalized distance of x/r. The magnitude of the velocity U_x is significantly lower than the magnitude of the velocity U_z. Approaching the jet exit, x/r $\rightarrow$ 1, U_x goes to zero and maintains a zero velocity within the jet. This decrease in the velocity of U_x is expected as the direction of jet thrust coincides with the z direction. With increasing motor speed, corresponding to an increase in body speed, the magnitude of U_x decreases. In the results for the second motor speed, figure 5.5(b), there are similarities in the velocity profile of U_x except for deviations after x/r $>$ 1.4. The normalized velocity of U_x sharply decreases to a value of 0.015 for the pulsed jet configuration whereas the normalized velocity of U_x gradually decreases to a value of 0.028 for the steady jet configuration. As the motor speed increases for the pulsed jet configuration, figure 5.5(c), U_x/U_{avg} maintains a relatively constant value of 0.011 for x/r $>$ 1. The normalized value of U_x is not constant for the steady jet configuration and reaches a maximum value of 0.025 for x/r = 1.1. In general, the magnitude of the normalized value of U_x was higher for the steady jet in comparison to the pulse jet. Note that the body speed achieved a higher magnitude for the pulsed jet in comparison to the steady jet with an equivalent jet speed. It is evident that with increased body speed, the magnitude of U_x decreases. The profile of U_x/U_{avg} obtained for the steady jet case in figure 5.5(b) is similar to the pulsed jet profile of U_x in figure 5.5(c). Both cases achieve comparable body speeds.

In figure 5.6, the root-mean-square velocity fluctuation in U_x, u$'$, is normalized by U_{avg} and is plotted against x/r. The velocity fluctuations are greater inside the jet in comparison to the fluctuations in the free stream. As the motor speed increases, there is a corresponding decrease in the velocity fluctuations outside the jet exit. The magnitude of the velocity fluctuations are on the order of the magnitude of the velocity of U_x.

5.4.2 Measurement of Entrainment Ratio for Both Steady and Unsteady Jet Propulsion with Equivalent Jet Speeds

To quantify the amount of entrained ambient fluid in the jet, the streamwise entrainment ratio was measured for both the steady and unsteady configuration. Figure 5.7 illustrates the relationship between the entrainment ratio and the motor speed. As the motor speed increases, there is a similar decrease in the entrainment ratio for both modes of propulsion. Krueger (2006) states that as the ratio of U_v/U_{avg} increases, the formation of the vortex ring process is preempted by the increased ring velocity as a result of convection from the coflow. This hampers the fluid entrainment into the vortex. The magnitude of the entrainment ratio is smaller for the steady jet mode of propulsion in comparison to the pulsed jet mode of propulsion for comparable motor speeds. The pulsed jet produces a 5.87% greater entrainment ratio at a motor speed of 2970 rpm over the steady jet at a motor speed of 2900 rpm. Although the pulsed and steady jet achieve a comparable jet speed at this motor speed, the measurement of the Froude efficiency for the pulsed jet was 26.13 and 6.58% higher than that of the steady jet. The increase in the total hydrodynamic efficiency for the pulsed jet was 11.2% when compared to the steady jet. This increase in propulsive performance supports the proposed benefits of increased ambient fluid entrainment due to vortex ring formation. A similar result was demonstrated at the higher motor speed. The pulsed jet produced a 5.22% greater entrainment ratio over the steady jet at an equivalent jet speed of 157 cm/s. The Froude efficiency was 6.45% higher for the pulsed jet configuration in comparison to the steady jet. The total efficiency measured was 10.79% higher for the pulsed jet configuration. The percentage difference in the measured entrainment ratio does not completely account for the difference in the measured propulsive efficiencies, however, only the benefits of increased entrainment at one particular z/d location have been taken into account. Table 5.1 summarizes the results obtained from the entrainment studies.

The measurement of the ambient fluid entrainment was obtained at only one axial position. As the vortex ring evolves and continues to roll up into a fully developed vortex ring, ambient fluid will continue to entrain into the vortex. The entrainment is constant in the far field of self-similar jets. In the near field, it must increase from zero at the nozzle to its final rate. Work supported

Table 5.1. Summary of entrainment studies for both pulsed and steady jet propulsion

Configuration	Motor Speed (rpm)	σ_{RPM}	U_{avg} (cm/s)	σ_{Uavg} (cm/s)	U_v (cm/s)	σ_{Uv} (cm/s)	η_{Froude} (%)	$\sigma_{\eta Froude}$ (%)	η_{Hydro} (%)	$\sigma_{\eta Hydro}$ (%)	Q_o (cm^3/s)	Q (cm^3/s)	Q / Q_o
Pulsed Jet	3200	29	158	30	32.8	5.0	34.4	6.47	43.16	7.28	2854.40	3186.31	1.12
	2970	28	149	30	22.3	4.8	26.13	5.58	31.42	6.71	2692.26	3041.99	1.13
	2750	29	142	32	13.9	5.1	17.81	5.36	20.04	6.73	2567.76	2944.18	1.15
Steady Jet Without Rotating Shell	3160	27	157	38	25.6	6.1	27.95	7.17	32.37	7.42	2848.06	2995.34	1.05
	2900	36	154	38	16.7	6.1	19.55	6.70	20.22	7.76	2790.70	3036.13	1.09

by Reynolds et al. (2003), Liepmann and Gharib (1992), and Ho and Gutmark (1987) indicate a monotonically increasing entrainment rate in the near field of the jet for values of z/d $<$ 10. Further measures of the entrainment ratio at higher z/d ratios are necessary to determine if a similar trend exists in the pulsed jet vehicle. A further increase in the entrainment ratio for the pulsed jet over the steady jet may become evident. The added mass effect may also play a role in increasing propulsive performance. This concept will be discussed in section 5.5.

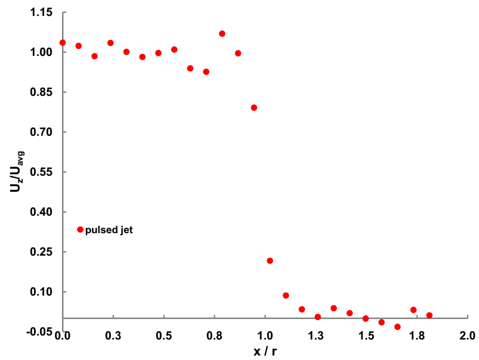

(a) Motor speed = 2750 rpm, U_{avg} = 142 cm/s.

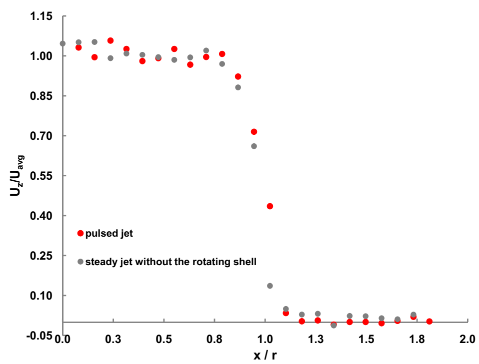

(b) Pulsed jet motor speed = 2970 rpm with U_{avg} = 149 cm/s, Steady jet motor speed = 2900 rpm with U_{avg} = 154 cm/s.

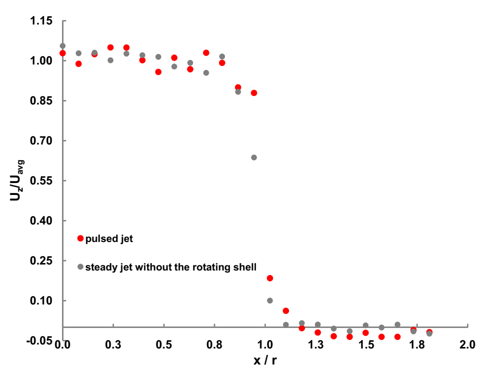

(c) Pulsed jet motor speed = 3200 rpm with U_{avg} = 158 cm/s, Steady jet motor speed = 3160 rpm with U_{avg} = 157 cm/s.

Figure 5.3. Variation of axial jet velocity U_z with translational distance in the x direction.

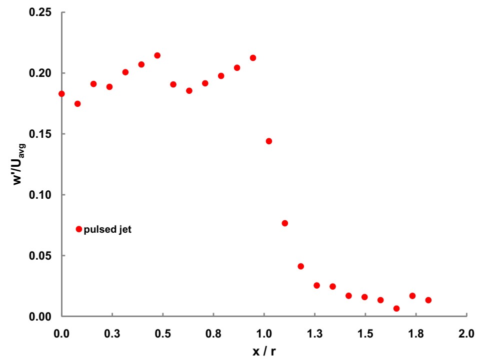

(a) Motor speed 2750 rpm, U_{avg} = 142 cm/s.

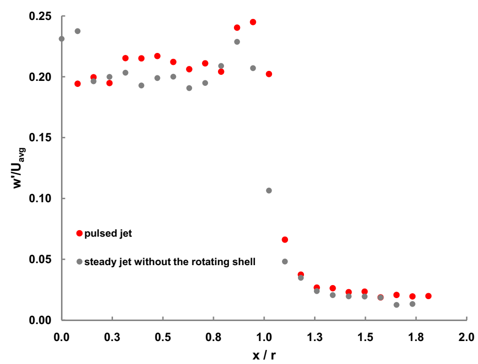

(b) Pulsed jet motor speed = 2970 rpm with U_{avg} = 149 cm/s, Steady jet motor speed = 2900 rpm with U_{avg} = 154 cm/s.

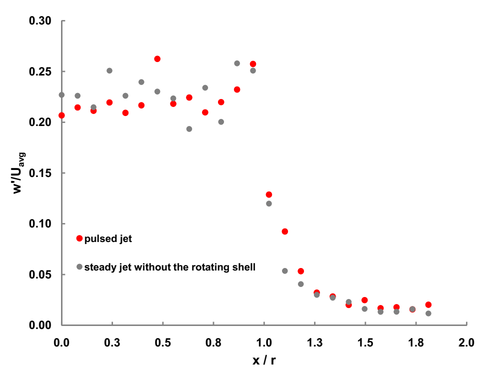

(c) Pulsed jet motor speed = 3200 rpm with U_{avg} = 158 cm/s, Steady jet motor speed = 3160 rpm with U_{avg} = 157 cm/s.

Figure 5.4. Variation of axial velocity fluctuations w′ with translational distance in the x direction.

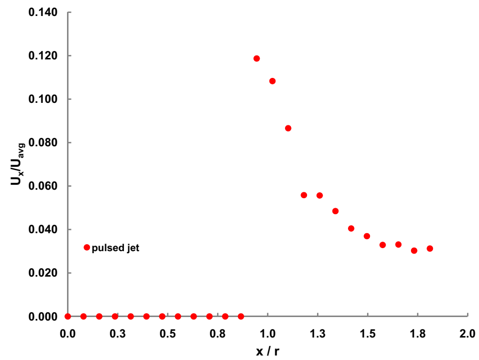

(a) Motor speed = 2750 rpm, U_{avg} = 142 cm/s.

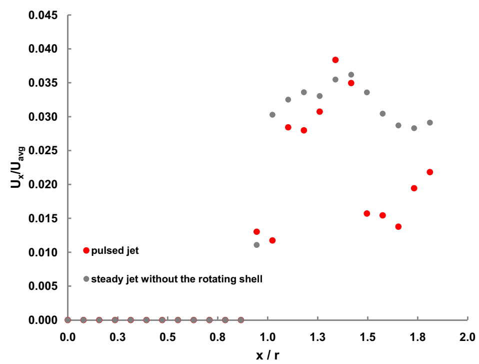

(b) Pulsed jet motor speed = 2970 rpm with U_{avg} = 149 cm/s, Steady jet motor speed = 2900 rpm with U_{avg} = 154 cm/s.

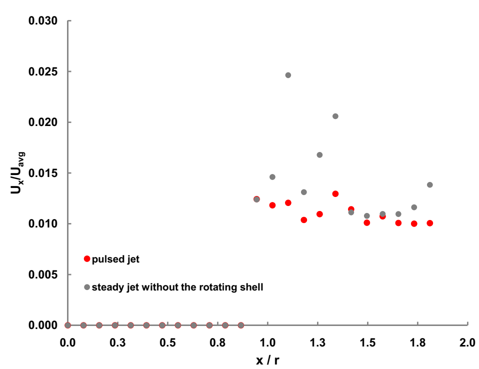

(c) Pulsed jet motor speed = 3200 rpm with U_{avg} = 158 cm/s, Steady jet motor speed = 3160 rpm with U_{avg} = 157 cm/s.

Figure 5.5. Variation of jet velocity U_x with translational distance in the x direction.

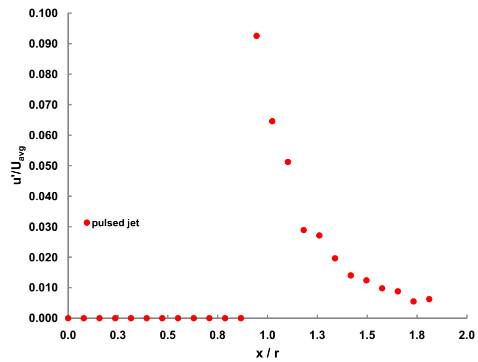

(a) Motor speed = 2750 rpm, U_{avg} = 142 cm/s.

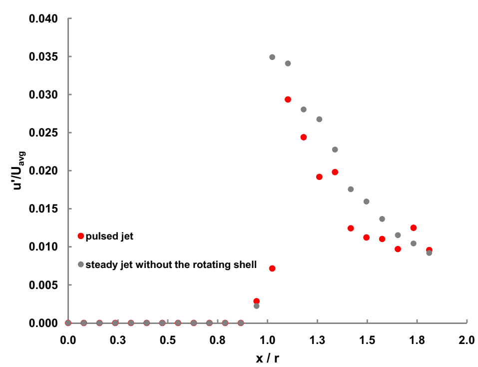

(b) Pulsed jet motor speed = 2970 rpm with U_{avg} = 149 cm/s, Steady jet motor speed = 2900 rpm with U_{avg} = 154 cm/s.

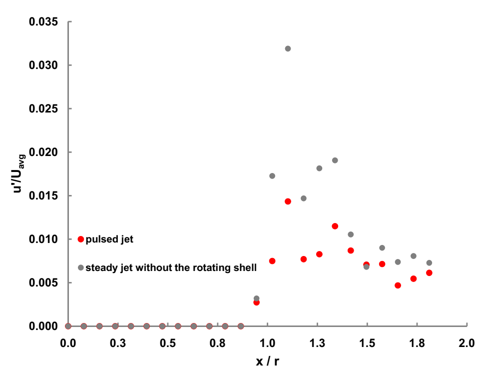

(c) Pulsed jet motor speed = 3200 rpm with U_{avg} = 158 cm/s, Steady jet motor speed = 3160 rpm with U_{avg} = 157 cm/s.

Figure 5.6. Variation of velocity fluctuations u′ with translational distance in the x direction.

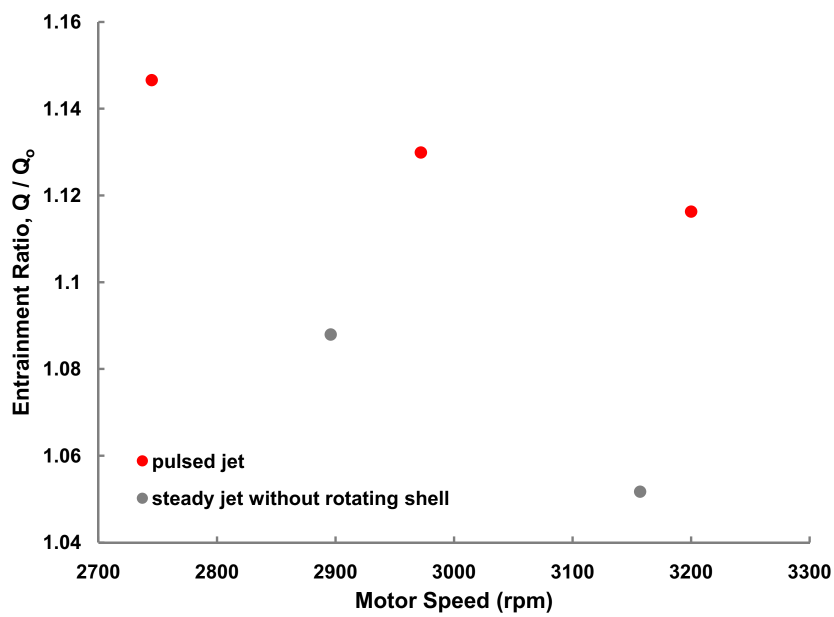

Figure 5.7. Relationship between entrainment ratio and motor speed.

5.5 Model of Proposed Contribution of Added Mass to Propulsive Performance

The second benefit of vortex ring formation for propulsion arises from the added mass effect which was described in section 5.3. In Krueger (2001), a model is presented for the initial stages of pulse ejection to determine an analytical evaluation of I_p. Added mass effects should dominate at the initiation of a pulse as the jet must initially push ambient fluid out of the way as it is ejected. The flow for x > 0 appears similar to the potential flow in front of a circular disk translating at a velocity U_{max} in the x direction. U_{max} is the maximum velocity of $U_J(t)$ over the interval of a pulse. The added mass associated with the flow in front of a circular disk is $m_{disk} = \frac{1}{6}\,\rho\,D^3$ (see section 6.10 of Batchelor (1967)). The impulse required to initiate the flow is given by equation (5.4).

$$I_p(t) \approx I_p(0) = m_{disk}\,U_{max} = \frac{1}{6}\,\rho\,D^3\,U_{max} \tag{5.4}$$

A few assumptions are made in determining an analytical solution for I_p. During the initial stage when the flow is being ejected from the nozzle, it appears more cylinder-like than ringlike for values of x/D << 1. The model ignores the roll up of the vortex ring and the unsteady component of the flow following the initiation of the jet. As a result of this assumption, entrainment is ignored along with the increasing effective diameter of the front of the slug. The model underestimates the contribution of pressure to $I_p(t)$ for t > 0.

To determine if the added mass effect associated with the acceleration of ambient fluid at the initiation of a starting jet can supply a substantial fraction of the pressure impulse, equation (5.4) was used to approximate the ratio $I(t)/I_p(t)$ for the three pulsed jet experiments that were conducted in the entrainment studies. The total impulse was calculated for the duration of a pulse and is defined by equation (5.5).

$$I \equiv \overline{T_p}\,t_p, \tag{5.5}$$

where $\overline{T_p}$ is the average thrust generated during a pulse. For steady state conditions, the thrust force is equivalent to the drag force, thus, the measure of $\overline{T_p}$ was obtained from the drag experiments as discussed in section 3.4.5. A summary of the results are displayed in table 5.2. As the motor speed increases, the ratio of $I_p(t)/I(t)$ slowly decreases as shown in figure 5.8. At the lowest motor speed, the estimated pressure impulse is 7% of the total impulse. This value decreases to 6.5% of the total impulse at the highest motor speed tested. The pressure impulse supplied to the flow due to the added mass effect provides an additional source for the increased proplusive performance that was observed in the pulsed jet mode of propulsion. Note that the estimated value obtained for $I_p(t)$ is an underestimate as the model does not account for the added mass effects associated with the change in the shape of the ring from a disc to an ellipsoid of larger diameter. The result demonstrates that the added mass effect associated with the acceleration of ambient fluid at the initiation of a starting jet provides an increase in the total impulse and is a source for increased propulsive performance.

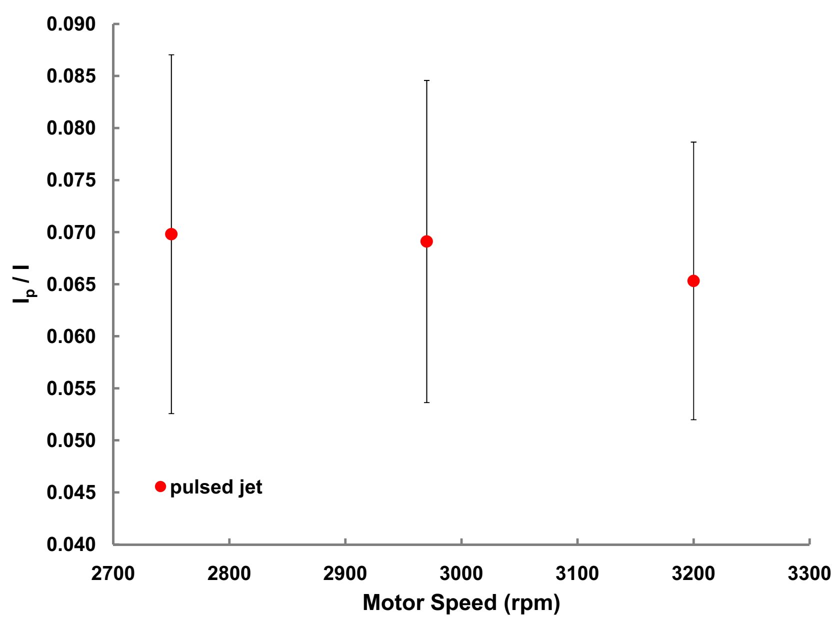

Figure 5.8. Relationship between $I_p(t)/I(t)$ and motor speed.

Table 5.2. Summary of parameters used in estimation of pressure impulse model

Configuration	Motor Speed (rpm)	U_{max} (cm/s)	U_v (cm/s)	t_p (s)	Drag (N)	I (Ns)	Model I_p (Ns)	I_p/I
Pulsed Jet	3200	162	32.77	0.09	5.77	0.541	0.035	0.065
	2970	157	22.33	0.10	4.92	0.496	0.034	0.069
	2750	149	13.87	0.11	4.25	0.465	0.032	0.070

5.6 Model of Proposed Contribution of Pressure Impulse to Propulsive Efficiency

Due to vortex ring formation, the additional acceleration of ambient fluid in the form of entrained and added mass results in an increase in the total fluid impulse. A model was developed to investigate how the increase in total fluid impulse relates to the propulsive efficiency. Recall that the total hydrodynamic efficiency as discussed in section 4.4.3 is equal to the following.

$$\eta_{hydro} = \frac{T\,U_v}{T\,U_v \;+\; \frac{1}{2}\rho\,A_j\,U_{avg}\,(U_{avg} - U_v)^2} \tag{5.6}$$

Provided that the system is traveling at steady state, the thrust produced by the system is equivalent to the drag. As discussed in section 5.5, the total impulse for the duration of a pulse is equal to the product of the average thrust generated during a pulse, $\overline{T_p}$, and the pulse duration, t_p. As shown in section 5.3, the total impulse can also be written as equation (5.2). Equating these two expressions and solving for $\overline{T_p}$, the following equation is obtained.

$$\overline{T_p} = \frac{W}{t_p}(m_{ejected} + m_{entrained} + M) \tag{5.7}$$

Equation (5.7) can be further broken down. The mass of fluid ejected from the nozzle during the pulse duration, $m_{ejected}$, is equal to $t_p\,\rho\,A_j\,U_{avg}$. The mass entrained into the developing vortex ring, can be approximated as $t_p\,\rho Q_{avg}$. The average measurement of the volumetric flow rate (Q_{avg})

during the pulse duration is used to prevent on overestimate of the contribution of $m_{entrained}$ to $\overline{T_p}$ given that the mass of the entrained fluid increases over the pulse duration. The added mass of the vortex ring, M, is approximated as the product of the added mass coefficient of the fully developed vortex ring, C_{AM}, and the total mass the vortex ring, $(m_{ejected} + m_{entrained})$. This approximation leads to an overestimate of the added mass force as the model does not account for the added mass effects associated with the change in the shape of the ring from a disc to an ellipsoid of larger diameter. At early stages, for values of z/D << 1, the jet initially appears similar to a disk with a diameter approximately equal to the jet exit diameter, Krueger (2001). As the vortex grows and develops into a fully developed vortex ring, the shape of the vortex becomes ellipsoidal and the added mass is increased. The added mass coefficient of an ellipsoid can be found in Milne-Thomson (1960). Krueger et al. (2006) cites that the vortex ring velocity, W, in the presence of uniform background coflow, can be approximated by equation (5.8). In this experiment, the coflow is generated by the motion of the vehicle, U_v.

$$W \approx \frac{1}{2}\left(U_{avg} + U_v\right) \tag{5.8}$$

This vortex ring velocity expression ignores the effect of the overpressure at the nozzle exit plane developed during the unsteady ring formation process but still provides a reasonable approximation (Krueger et al. 2006).

Taking the approximations for $m_{ejected}$, $m_{entrained}$, and W and plugging their results into equation (5.7), the following equation is generated.

$$\overline{T_p} = \frac{1}{2}\left(U_{avg} + U_v\right)\left[\left(\rho\, A_j\, U_{avg} + \rho\, Q_{avg}\right)\left(1 + C_{AM}\right)\right] \tag{5.9}$$

Taking the result developed for $\overline{T_p}$ in equation (5.9) and substituting into equation (5.6) for T, the following definition for propulsive efficiency is developed.

$$\eta_{model} = \frac{\frac{U_v}{2}\,(U_{avg}+U_v)\,[(\rho\, A_j\, U_{avg} + \rho\, Q_{avg})\,(1+C_{AM})]}{\frac{U_v}{2}\,(U_{avg}+U_v)\,[(\rho\, A_j\, U_{avg} + \rho\, Q_{avg})\,(1+C_{AM})]\;+\;\frac{1}{2}\rho\, A_j\, U_{avg}\,(U_{avg}-U_v)^2} \tag{5.10}$$

This metric for propulsive efficiency clearly establishes a relationship between the propulsive efficiency, ambient fluid entrainment and added mass.

5.6.1 Measurement of Propulsive Efficiency Using Estimated Total Impulse

The model was applied to estimate the propulsive efficiency for the pulsed jet configuration at the three motor speeds described in 5.2. Since the measurement of the ambient fluid entrainment was obtained at only one axial position, z/r = 0.5, the value of Q_{avg} was estimated using a linear fit. In previous work, Reynolds et al. (2003), Liepmann and Gharib (1992), and Ho and Gutmark (1987), the mass of the entrained fluid into the vortex has been shown to approximately equal zero at the nozzle exit and increase linearly as the vortex develops and moves downstream for values of z/d < 10. A linear curve fit for the ratio of $Q_{entrained}/Q_o$ versus downstream distance was developed. $Q_{entrained}$ is the volumetric flow rate of the entrained flow into the wake and is calculated by subtracting Q_o from Q.

To calculate Q_{avg}, the position of the vortex ring at the end of the pulse duration (z_{tp}) is required and was estimated by $z_{tp} \approx W\, t_p$. The value of z_{tp}/r is substituted into the corresponding equation based on motor speed as shown in figure 5.9 and is used to estimate the ratio of $Q_{entrained}/Q_o$ at the end of the pulse duration. The value of Q_{avg} is estimated as $Q_{entrained}/2$ given the linear relationship between $Q_{entrained}/Q_o$ and downstream distance. The results for the measurement of Q_{avg}, W and t_p are summarized in Appendix F.

Substituting for Q_{avg} in equation 5.10, equation 5.11 is obtained.

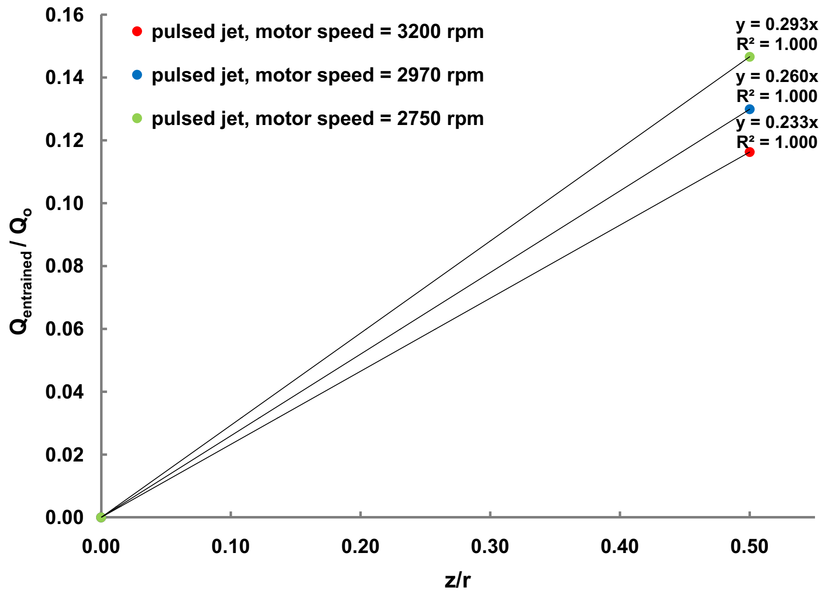

Figure 5.9. Plot of ambient fluid entrainment as a function of downstream distance for three motor speeds.

$$\eta_{model} = \frac{\frac{U_v}{2}\,(U_{avg}+U_v)\,[(\rho\,A_j\,U_{avg}+\rho\,\frac{Q_{entrained}}{2})\,(1+C_{AM})]}{\frac{U_v}{2}\,(U_{avg}+U_v)\,[(\rho\,A_j\,U_{avg}+\rho\,\frac{Q_{entrained}}{2})\,(1+C_{AM})]\;+\;\frac{1}{2}\rho\,A_j\,U_{avg}\,(U_{avg}-U_v)^2} \tag{5.11}$$

The first step in estimating C_{AM} was to calculate the formation time. Given that the geometry of the vortex ring during development is unknown, C_{AM} was estimated indirectly using data of vortex ring geometry from PLIF experiments in Krueger (2001) and from DPIV experiments obtained from Shadden et al. (2007). Supporting data for vortex rings of a comparable formation time was used to estimate the geometry of the fully developed vortex ring. The formation time was approximately 3 for all motor speeds. The vortex ring geometry was estimated using the formation time and C_{AM} was calculated using the added-mass coefficient of an ellipsoid (Milne-Thomson 1960) and found to be 0.72. Using the value of C_{AM} for a fully developed vortex leads to an overestimate in the measurement of the added mass for the duration of the pulse and consequently an overestimate in $\overline{T_p}$. Due to the unavailability of vortex ring geometry data at a corresponding coflow velocity ratio (U_{avg}/Uv) and formation time, the geometry of the vortex was determined from previous experiments without the presence of a coflow velocity. Krueger et al. (2006) states that the vortex ring formation process is preempted by the increased ring velocity as a result of convection from the coflow, thereby decreasing the size of the vortex ring in comparison to the case without the presence of the coflow. This result of a decrease in vortex ring size due to the presence of the coflow has not be taken into account in the estimate of C_{AM} and may also lead to a further overestimate in $\overline{T_p}$.

The results for estimated propulsive efficiency obtained using equation (5.11) for the three motor speeds are found in Appendix F. The model is sensitive to the value of C_{AM}. Initially the value of C_{AM} was estimated to be the value for a fully developed vortex which led to a higher value of η_{hydro} modeled in comparison to the experimental value of η_{hydro}, see figure 5.10. At the early stages of vortex ring formation the flow being ejected from the nozzle appears more cylinder like than ring like. Choosing a value of C_{AM} for a circular disk, leads to a lower value of η_{hydro} modeled in comparison to the experimental value of η_{hydro}. Using the estimated value of C_{AM} as the shape of a fully developed vortex ring and the shape of a circular disk bound the experimental measurement of η_{hydro}. These results justify the increase in propulsive efficiency for the pulsed jet configuration in comparison to the steady jet configuration due to the increase in thrust production generated by entrained and added mass forces developed during vortex ring formation. Provided that the values of Q_{avg} and C_{AM} can be estimated, this model serves as another metric for determining the propulsive efficiency of a system. It should be noted that as motor speed increases, the ratio of $I_p(t)/I(t)$ slowly decreases as shown in figure 5.8, therefore contributing less to the generation of overpressure at the nozzle exit. An eventual decrease in the overpressure due to increased motor speed will decrease the amount of useful work provided for propulsion and may exhibit a propulsive efficiency comparable to the steady jet configuration. As motor speed increases, the time between fluid pulses decreases, leading to increased vortex interactions. Krueger (2005) has shown that increasing pulsing duty cycle increases the vorticity from preceding pulses near the nozzle at the ejection of each pulse. This behavior requires less fluid to be accelerated by the issuing pulse and reduces nozzle exit overpressure.

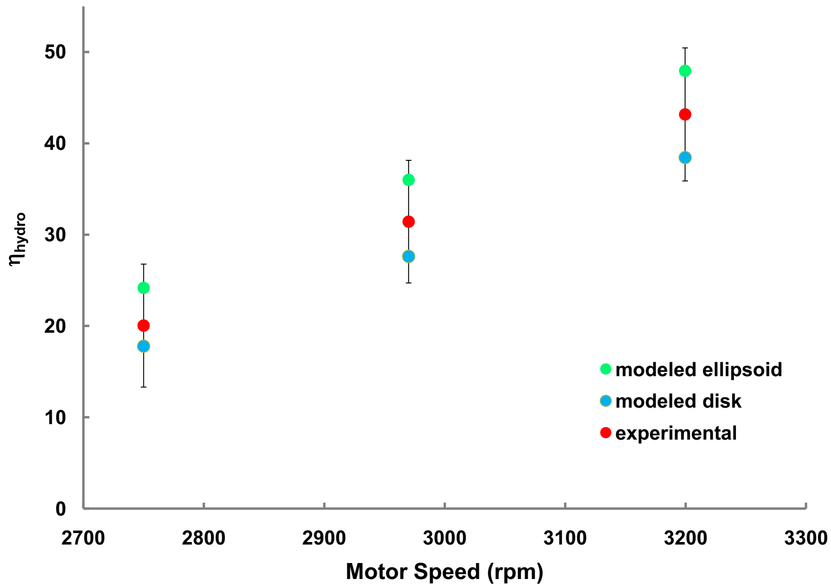

Figure 5.10. Illustration of accuracy of model in estimating propulsive efficiency.

5.7 Conclusion

This chapter discussed the potential sources that contributed to increased propulsive performance. Analysis demonstrates that the acceleration of two classes of ambient fluid can led to an increase in propulsive performance. The first source of ambient fluid acceleration investigated was that of entrained mass that is inducted into the body of the ring as the shear layer rolls up and is convected downstream with the ring. To quantify the amount of entrained ambient fluid into the jet, the streamwise entrainment ratio was measured for both the steady and unsteady jet. The entrainment ratio was measured for two motor speeds in the steady jet configuration and three motor speeds in the pulsed jet configuration. To obtain a measurement of the entrainment ratio, the velocity profile of the jet was measured. The axial jet velocity profiles were similar to a top hat for both the steady and pulsed jet modes of propulsion and for all motor speeds tested. These profiles are similar to the work of Reynolds et al. (2003) and Ho and Gutmark (1987). The magnitude of the velocity outside the jet was greater for the pulsed jet in comparison to the steady jet for a given equivalent jet speed suggesting increased fluid entrainment due to vortex ring formation.

The velocity profiles for U_x were also measured for three different motor speeds. The magnitude of the velocity U_x is significantly lower than the magnitude of the velocity U_z. As x/r approaches the jet exit, the value of U_x went to zero and maintained a zero velocity within the jet. The decrease in the velocity of U_x was expected as the direction of jet thrust coincided with the z direction. With increasing motor speed and a corresponding increase in body speed, the magnitude of U_x was shown to decrease. In general, the magnitude of the normalized value of U_x was higher for the steady jet in comparison to the pulsed jet. This result may be attributed to the pulsed jet configuration acquiring a higher body speed in comparison to the steady jet configuration with an equivalent jet speed. The root-mean-square velocity fluctuation in U_x, u$'$, was also calculated. The velocity fluctuations were shown to be greater inside the jet in comparison to the fluctuations in the free stream. As the motor speed increased, there was a corresponding decrease in the velocity fluctuations outside the jet exit. The magnitude of the velocity fluctuations were on the order of the magnitude of the velocity U_x.

The measured streamwise entrainment ratio was shown to decrease with increased motor speed for both modes of propulsion. The magnitude of the entrainment ratio was smaller for the steady jet mode of propulsion in comparison to the pulsed jet mode of propulsion at comparable motor speeds. The pulsed jet produced a 5.87% greater entrainment ratio at a motor speed of 2972 rpm over the steady jet at a motor speed of 2896 rpm. Despite both configurations achieving comparable jet speeds at this motor speed, the measured Froude efficiency for the pulsed jet was 26.13 and 6.58% higher in comparison to the steady jet. The increase in the total hydrodynamic efficiency for the pulsed jet was 11.2% over the steady jet. A similar result was demonstrated at the higher motor speed. The percentage difference in the measured entrainment ratio does not completely account for the difference in the measured propulsive efficiencies. However, only the benefit of increased entrainment at one z/d location has been measured and taken into account. A further increase in the entrainment ratio for the pulsed jet compared to the steady jet may be evident at higher z/d ratios. Work supported by Reynolds et al. (2003), Liepmann and Gharib (1992), and Ho and Gutmark (1987) indicate a monotonically increasing entrainment ratio in the near field of the jet for values of $z/d < 10$. Further measures of the entrainment ratio at higher z/d ratios are necessary to determine if a similar trend exists with the pulsed jet vehicle.

The role of the added mass effect was investigated for the purpose of increasing propulsive performance. The total impulse in the flow was shown to increase with the presence of vortex ring formation due to nozzle-exit overpressure. A model developed by Krueger (2001) is used to determine the fraction of the total impulse imparted to the flow that is contributed to by added mass. As the motor speed increased, the ratio of $I_p(t)/I(t)$ slowly decreased. At the lowest motor speed, the estimated pressure impulse was 7% of the total impulse and decreased to 6.5% of the total impulse at the highest motor speed. The result demonstrates that the added mass effect associated with the acceleration of ambient fluid at the initiation of a starting jet provides an increase in the total impulse and is thus a source for increased propulsive performance.

A metric for propulsive efficiency was developed to demonstrate the relationship between the propulsive efficiency, ambient fluid entrainment and added mass. The model is sensitive to the value of C_{AM}. Initially the value of C_{AM} was estimated to be the value for a fully developed vortex which led to a higher value of η_{hydro} modeled in comparison to the experimental value of η_{hydro}. Using the estimated value of C_{AM} as the shape of a fully developed vortex ring and the shape of a circular disk bound the experimental measurement of η_{hydro}. These results justify the increased propulsive efficiency of the pulsed jet configuration in comparison to the steady jet configuration due to increased thrust production generated by the entrained and added mass force developed during vortex ring formation. Providing that the values of Q_{avg} and C_{AM} can be estimated, this model serves as another metric for determining the propulsive efficiency of a system. It should be noted that as motor speed increases, the ratio of $I_p(t)/I(t)$ slowly decreases, therefore contributing less to the generation of overpressure at the nozzle exit. An eventual decrease in the overpressure due to increased motor speed will decrease the amount of useful work provided for propulsion and may exhibit a propulsive efficiency comparable to the steady jet configuration. As motor speed increases, the time between fluid pulses decreases, leading to increased vortex interactions. Krueger (2005) has shown that increasing pulsing duty cycle increases the vorticity from preceding pulses near the nozzle at the ejection of each pulse. This behavior requires less fluid to be accelerated by the issuing pulse and reduces nozzle exit overpressure.